Available online at www.sciencedirect.com
SCIENCE DIRECT®
Journal of Luminescence 117 (2006) 13–19
JOURNAL OF LUMINESCENCE
www.elsevier.com/locate/jlumin

Measurement of the $^4F_{5/2}$ and $^2H(2)_{9/2}$ manifold lifetime in Nd^{3+}:$YLiF_4$

B.M. van der Ende[a], R.L. Brooks[a,*], H.F. Tiedje[b], Hong Sun[b,1], H.K. Haugen[b,2]

[a]*Guelph-Waterloo Physics Institute, University of Guelph, 50 Stone Road East, Guelph, Ontario, Canada N1G 2W1*
[b]*Brockhouse Institute for Materials Research, McMaster University, 1280 Main Street West, Hamilton, Ontario, Canada L8S 4M1*

Received 9 February 2005
Available online 10 May 2005

Abstract

We present direct measurements of the lifetime of the $^4F_{5/2}$ and $^2H(2)_{9/2}$ manifold in Nd^{3+}:$YLiF_4$, using a fluorescence pump–probe technique. The technique populates the $^4F_{5/2}$ and $^2H(2)_{9/2}$ manifold directly with a pump pulse. Via excited state absorption from this excited manifold, the $^2F(2)_{5/2}$ manifold of Nd^{3+} is populated with a delayed probe pulse. The population in the $^4F_{5/2}$ and $^2H(2)_{9/2}$ manifold is monitored as a function of time by observing the change in integrated UV fluorescence from the $^2F(2)_{5/2}$ manifold for each time delay between pump and probe pulses. The pump (~780 nm) and probe (~390 nm) beams come from the fundamental and second harmonic wavelengths of a femtosecond Ti:sapphire regenerative amplifier. The measured lifetime (230 ± 30 ps) agrees well with the energy gap law, based on other nonradiative lifetime measurements from the literature for Nd^{3+}:$YLiF_4$.

PACS: 78.47.+p; 78.20.−e; 42.70.Hj

Keywords: Nd^{3+}:$YLiF_4$; Pump–probe spectroscopy; UV fluorescence; Nonradiative relaxation; Energy gap law

1. Introduction

Four-level laser schemes involve pumping from a ground state level to a pump band, which then decay rapidly to a metastable upper laser level. This upper level lases to a lower level that in turn decays quickly to the ground state. In such a system, the relaxation of the pump band to the metastable level should be fast compared to the fluorescence decay time of the metastable level.

*Corresponding author. Tel.: +1519 824 4120; fax: +1519 836 9967.
E-mail address: rbrooks@uoguelph.ca (R.L. Brooks).
[1]Currently at University of California, Los Angeles, CA, USA 90095.
[2]Also with the Departments of Physics and Astronomy, and Engineering Physics, McMaster University.

0022-2313/$ - see front matter © 2005 Elsevier B.V. All rights reserved.
doi:10.1016/j.jlumin.2005.03.013

Further, this pump band relaxation rate needs to be much faster than the pump band fluorescence to any other level [1].

The $^4F_{5/2}$ and $^2H(2)_{9/2}$ manifold serves as a pump band in diode-pumped Nd^{3+} solid-state lasers using the $^4F_{3/2}$ metastable state as the upper laser level. Semiconductor diode lasers typically pump at ~808 nm, to directly excite the $^4F_{5/2}$ and $^2H(2)_{9/2}$ manifold [2,3]. The $^4F_{5/2}$ and $^2H(2)_{9/2}$ manifold typically lies ~900 cm^{-1} (938 cm^{-1} in $YLiF_4$) above the $^4F_{3/2}$ laser level. This energy gap can usually be spanned by 2–3 effective phonon energies (or less) of the dielectric host, so the mechanism for relaxation from the former manifold is primarily nonradiative [4].

Multiphonon nonradiative relaxation in rare-earth-doped dielectric solids has been extensively studied since the 1960s. There are review publications which provide access to the considerable literature found on this topic [1,4–8]. The phenomenological energy gap law has been used to correlate the nonradiative decay rate $W_{jj'}$ of a given 4f level with the size of the energy gap $\Delta E_{jj'}$ between that manifold and the next manifold lower in energy. Kaminskii [8] writes the basic relation as

$$W_{jj'} = B\exp(-\beta\Delta E_{jj'})[1-\exp(-\hbar\omega/kT)]^{-p}, \quad (1)$$

where $\hbar\omega$ is the effective phonon energy of the dielectric host, and $p = \Delta E_{jj'}/\hbar\omega$ is the number of phonons spanning the energy gap. The values of B and β are host dependent, and are assumed to be independent of the nature of the 4f states of the rare earth ion as well as the vibronic modes of the host. The phonon energy is generally taken to be an effective energy that can be equal to or less than the energy of the highest-frequency optical phonon in the crystal host vibration spectrum. Riseberg and Weber [4] point out that the validity of this single-frequency model is dependent on how well the individual features of the phonon modes and electronic states are statistically averaged out in the multiphonon process. This basic model has had considerable success in describing the trend of experimentally measured nonradiative decay times. Some authors have modified Eq. (1) through theoretical arguments by replacing $\Delta E_{jj'}$ with $\Delta E_{jj'} - 2\hbar\omega$ [9,10] or $\Delta E_{jj'} - 2.6\hbar\omega$ [11,12], with the observation that such modifications result in reduced variation in B from crystal host to crystal host. Others [6,7,13] have sought to develop more detailed models of nonradiative decay. The nonlinear model due to Orlovskii et al. [7] has accounted for deviations from single-exponential dependence on energy gap, as observed in Nd^{3+}:$YLiF_4$ [7] and Nd^{3+}:YVO_4 [12].

Multiphonon decays are usually measured in two ways [1]. One way involves measuring the fluorescence decay rate $1/\tau_f$ of the level, and then subtracting the radiative decay rate $1/\tau_r$ via the relation

$$\frac{1}{\tau_f} = \frac{1}{\tau_{nr}} + \frac{1}{\tau_r}. \quad (2)$$

The radiative decay rate is usually calculated from absorption cross-sections, or from Judd–Ofelt theory. If the level does not fluoresce, however, then the second way of estimating $1/\tau_{nr}$ involves measuring the delayed rise of fluorescence from the terminal level of the nonradiative transition, and making use of appropriate kinetic models.

In more recent years, nonradiative relaxation rates have been measured using pump–probe arrangements. In some instances, absorption and gain recovery measurements provide the data in such arrangements [14–16], while in other cases fluorescence decay data coupled with kinetic modeling are used to estimate the nonradiative relaxation rates in such experiments [17,18].

In this paper, we measure the nonradiative decay rate of the $^4F_{5/2}$ and $^2H(2)_{9/2}$ manifold in Nd^{3+}:$YLiF_4$ (Nd:YLF), using a fluorescence pump–probe technique. The technique populates the $^4F_{5/2}$ and $^2H(2)_{9/2}$ manifold directly with a pump pulse (~780 nm). Via excited state absorption from this excited manifold, the $^2F(2)_{5/2}$ manifold of Nd^{3+} is populated with a delayed probe pulse (~390 nm). The population in the $^4F_{5/2}$ and $^2H(2)_{9/2}$ manifold is monitored as a function of time by observing the change in integrated UV fluorescence from the $^2F(2)_{5/2}$ manifold for each time delay between pump and probe pulses. The technique is described in detail in the following section.

2. Experimental methods

Fluorescence pump–probe experiments were performed on a single crystal sample of Nd:YLF, acquired from Alphalas GmbH (Goettingen, Germany). The Nd:YLF sample (1.1% at. doping) has a 7mm × 4 mm × 2 mm polished cut.

The pumping and fluorescence processes in our experiment for Nd:YLF is shown in Fig. 1, where we have used experimental energy levels from Ref. [19]. For simplicity, energy levels between the $^4F_{5/2}$ and $^2H(2)_{9/2}$ manifold and the $^2F(2)_{5/2}$ manifold have been omitted. The $^4F_{5/2}$ and $^2H(2)_{9/2}$ manifold is populated by a ~780 nm pump laser pulse, and subsequently the $^2F(2)_{5/2}$ manifold is populated by a ~390 nm probe laser pulse, excited from the $^4F_{5/2}$ and $^2H(2)_{9/2}$ manifold.

Fig. 2 shows the optical layout employed for the fluorescence pump–probe experiments. A regeneratively amplified 1 kHz femtosecond laser system (Spectra-Physics Spitfire LCX) is used to produce ~140 fs tunable pulses (~780 nm), with a bandwidth of 10 nm. A 1 mm thick beta barium borate (BBO) crystal is used to double the frequency

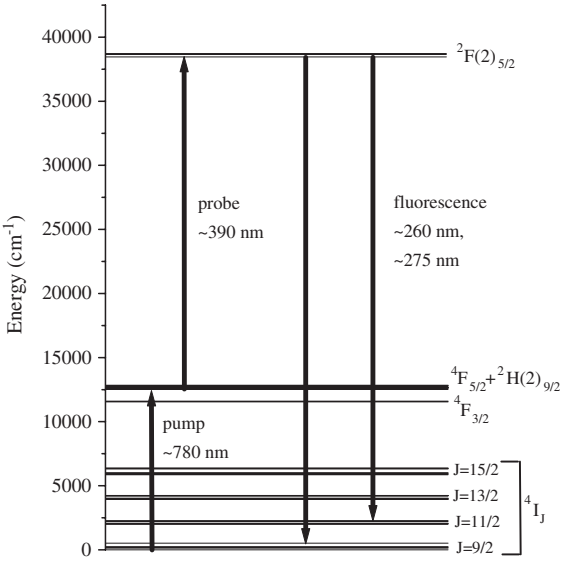

Fig. 1. Scheme of pump and probe excitation in Nd^{3+}, together with some of the possible emission processes that are monitored. The energy levels shown are those for Nd:YLF [19]. Levels between the $^4F_{5/2}$ and $^2H(2)_{9/2}$ manifolds, and the $^2F(2)_{5/2}$ manifold, are omitted for clarity.

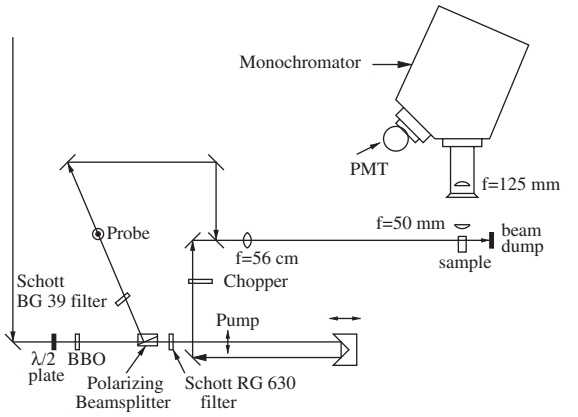

Fig. 2. Schematic optical layout for the fluorescence pump–probe experiments. Actual beams pass vertically through the sample, parallel to the monochromator entrance slit.

~780 nm pulses to create ~390 nm pulses with a bandwidth of 2 nm. The (orthogonally polarized) ~390 nm beam and residual ~780 nm beam are separated after the BBO crystal by a polarizing beam splitter into pump and probe beams. Schott glass filters are used to remove residual pump wavelength light from the probe beam, and to remove residual probe wavelength light from the pump beam. The pump beam is directed into a delay line, and is chopped at 500 Hz so that every other pump beam pulse is blocked by the chopper wheel. The pump and probe beams are recombined, and then traverse the crystal colinearly. Pulse energies for each beam incident at the crystal are typically 1–10 μJ/pulse. Inside the crystal sample, the pump and probe beams are focused to a $1/e^2$ diameter of ~175 μm. The path length of the beams within the Nd:YLF crystal sample is 4 mm.

A Stanford SR400 photon counter accepts the fluorescence signal detected by a solar-blind Hamamatsu R166UH side-on photomultiplier tube (PMT) through a 0.3 m, f/5.3, plane-grating monochromator (McPherson model 218; the slits on the monochromator are set to 1.2 mm wide in this work, giving 3 nm spectral resolution). Gate A of the photon counter is timed to measure signal with pump and probe beams together through the crystal, while gate B is timed to measure signal with just the probe beam through the crystal. The

difference between the A and B signals is due to fluorescence resulting from absorption of probe light from the excited $^4F_{5/2}$ and $^2H(2)_{9/2}$ manifold into the $^2F(2)_{5/2}$ manifold. The opening of gates A and B is delayed with respect to the laser pulses by 1–2 μs, so that scattered light and background $4f^25d$ fluorescence emission that is picked up by the PMT is not registered by the photon counter. (The $4f^25d$ configuration is reached by excited state absorption of two probe photons, or by ground state absorption of three probe photons; $4f^25d \rightarrow 4f^3$ fluorescence, being spin and parity allowed, typically has a lifetime of tens of nanoseconds [20,21].) The equal time widths of gates A and B are set to 50 μs, which is about 5 times the ~10 μs fluorescence decay time measured for the $^2F(2)_{5/2}$ manifold of Nd:YLF [22,23].

3. Results and discussion

3.1. Fluorescence spectra

Fig. 3 shows the photon counter difference signal (A−B) as a function of wavelength for the Nd:YLF crystal sample. Each of the broad peaks seen in Fig. 3 can be assigned to transitions from the $^2F(2)_{5/2}$ manifold to each of the $^4I_{9/2}$, $^4I_{11/2}$, $^4I_{13/2}$, and $^4I_{15/2}$ manifolds of Nd^{3+}. A spectrum similar to Fig. 3 has also been reported for 532 nm 2-photon excitation of $^2F(2)_{5/2}$ at room temperature [24].

Kaminskii et al. [25] have calculated, using Judd–Ofelt theory, the branching ratios for $^2F(2)_{5/2}$ fluorescence in Nd:YLF. The branching ratios of the $^4I_{11/2}$, $^4I_{13/2}$, and $^4I_{15/2}$ transitions relative to the $^4I_{9/2}$ transition are predicted to be 0.12, 1.2, and 0.31, respectively. These predictions are in disagreement with the ratios observed in Fig. 3, which are 0.32, 0.35, and 0.036, respectively. Others have previously noted inaccurately predicted branching ratios, such as in Ref. [26]. The reason given in Ref. [26] for the discrepancy was a breakdown of one of the fundamental approximations used in deriving Judd–Ofelt theory. The assumption broken was that the initial and terminal manifolds of a given 4f–4f transition have the same energy difference with respect to the $4f^25d$ configuration of Nd^{3+}. This approximation is worse for the $^2F(2)_{5/2} \rightarrow {}^4I_J$ transitions observed in Fig. 3 than for the transitions studied in Ref. [26], and therefore is likely to be a large factor in the discrepancies from theory observed in Fig. 3.

3.2. Fluorescence decay curves

Fig. 4 shows typical $^2F(2)_{5/2}$ fluorescence emission as a function of pump–probe delay time. A

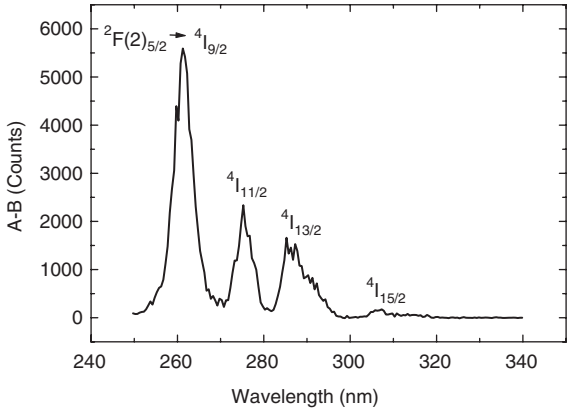

Fig. 3. Wavelength spectra of the emission difference signal recorded with the SR400 photon counter for Nd:YLF. In each case, the difference signal at each point is averaged over 1000 optical chopper cycles, at zero delay time between pump and probe pulses.

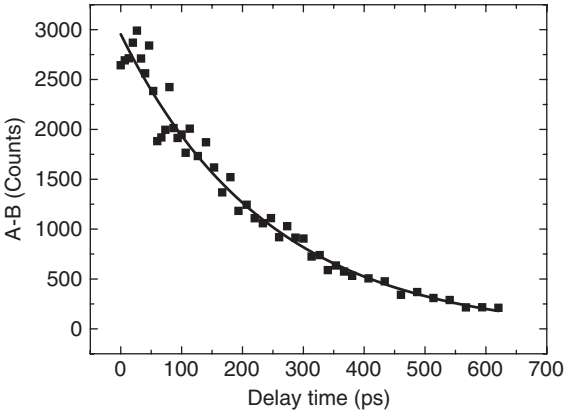

Fig. 4. Representative decay of difference signal A−B versus pump–probe delay time, together with corresponding single-exponential fit, for Nd:YLF (@260.7 nm; $^2F(2)_{5/2} \rightarrow {}^4I_{9/2}$). The difference signal at each point is averaged over 10000 optical chopper cycles.

single exponential decay model provides a good fit to the data. The decay lifetime measured from fitting this model to the data is the population lifetime in the $^4F_{5/2}$ and $^2H(2)_{9/2}$ manifold. Population decay from this manifold should be primarily nonradiative, as pointed out in the Introduction of this paper.

Our interpretation of the experiment implies single-photon absorption of each of the pump and probe beams. We have measured the difference signal A−B as a function of pump power, and of probe power. In each case, the scaling of the difference signal with the varied beam power is linear (see Fig. 5). This confirms the single-photon absorption of both pump and probe beams in these hosts. The nonzero y-intercepts seen in Fig. 5 are contributed to by some imprecision in the balancing of the A−B signal.

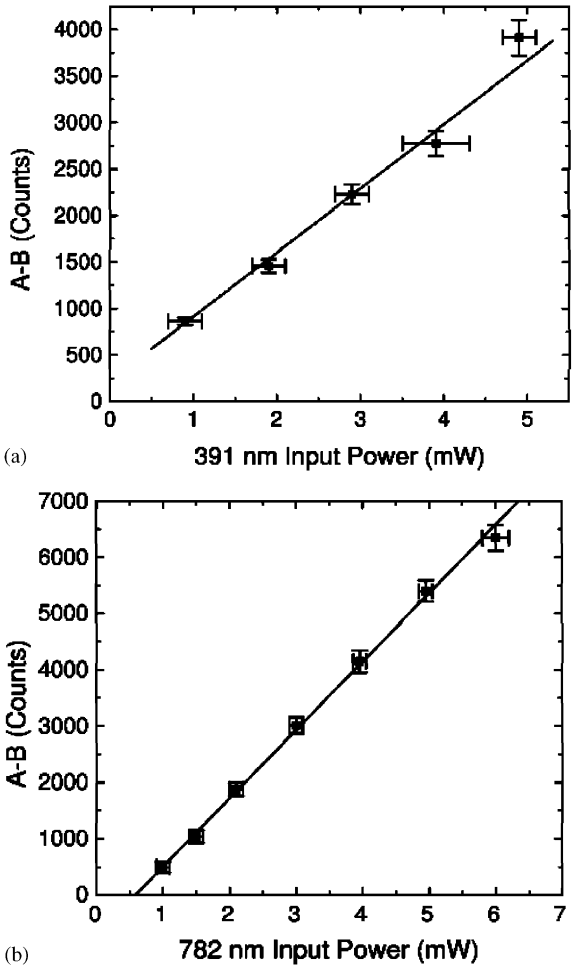

Fig. 5. Power dependence of A−B signal, as a function of (a) 391 nm input power (782 nm power held at 6.1 ± 0.5 mW), and of (b) 782 nm power (391 nm power held at 6.0 ± 0.3 mW).

To further verify our pumping scheme, we have measured the difference signal A−B as a function of probe (and corresponding pump) wavelength. The results for Nd:YLF are shown in Fig. 6. The signal at each wavelength was recorded at the same pump–probe delay time. In this plot, we have normalized the signal with respect to the pump and probe beam powers, as well as the absorption of the pump beam, which was estimated using a one-photon absorption curve. This normalization provides a spectrum of the probe beam absorption from the $^4F_{5/2}$ and $^2H(2)_{9/2}$ manifold to the $^2F(2)_{5/2}$ manifold. Fig. 6 shows that the normalized signal peaks at 388 nm. This matches the energy difference between the $^4F_{5/2}$ and $^2H(2)_{9/2}$ manifold and the $^2F(2)_{5/2}$ manifold [19]. This further confirms that the difference signal arises from excited state absorption of the probe beam from the $^4F_{5/2}$ and $^2H(2)_{9/2}$ manifold to the $^2F(2)_{5/2}$ manifold.

Table 1 summarizes the lifetimes acquired from single-exponential decay fits of various data sets: each entry in the table is for a specific data set. Each set monitored a certain fluorescence channel under a specific excitation wavelength. The table

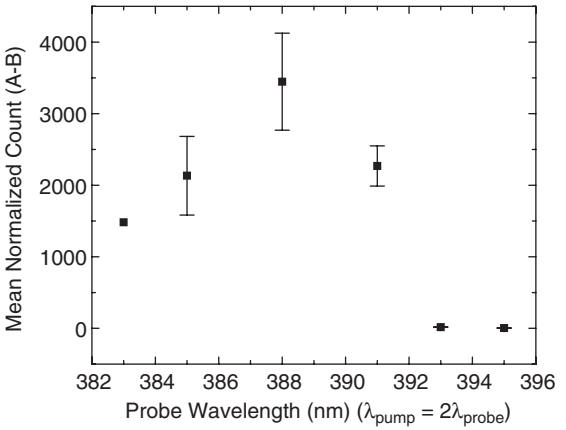

Fig. 6. Signal from Nd:YLF (at 260.7 nm; $^2F(2)_{5/2}\rightarrow{}^4I_{9/2}$) normalized by pump and probe input powers and pump absorption over the crystal path length (4 mm), as a function of probe wavelength.

Table 1
Summary of fit decay times

Fluorescence channel	$\lambda_{pump} + \lambda_{probe}$ (nm)	Decay time and error (ps)
$^2F(2)_{5/2} \rightarrow {}^4I_{11/2}$ (274.7 nm)	782 + 391	214 ± 17
		219 ± 15
$^2F(2)_{5/2} \rightarrow {}^4I_{9/2}$ (260.7 nm)	782 + 391	219 ± 18
		230 ± 19
	775 + 387.5	193 ± 17
		282 ± 24
	790 + 395	242 ± 19
		252 ± 16
Weighted mean, std. dev. (ps)		230 ± 30

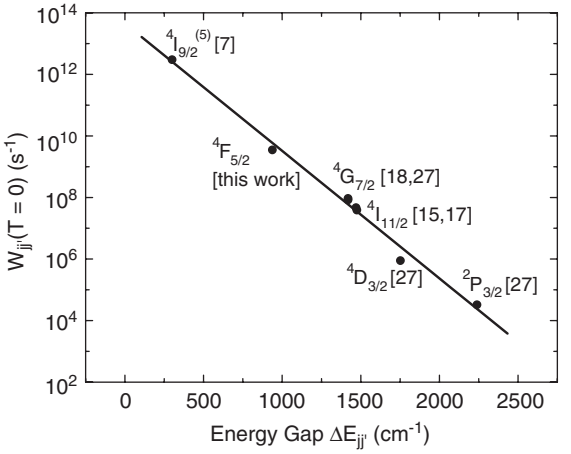

Fig. 7. Plot of experimental nonradiative decay rates for various states in Nd:YLF, as a function of the energy gap between the lowest splitting of the state and the highest splitting of the next lower state. References are cited for values from literature. ([27])

demonstrates that the decay rate is (within error) independent of the fluorescence channel and the excitation wavelength. The errors on the lifetimes are statistical estimates from the least-squares Marquardt method. An average lifetime weighted by these errors has been computed. The associated error quoted with this average is simply the standard deviation of all of the fit lifetimes for the host. The standard deviation can differ significantly from the statistical fit error estimates. This is due to significant correlation present between the A and B signal channels of the photon counter that is difficult to account for in the statistical fit error estimates.

3.3. Comparing experimental results via the energy gap law

Fig. 7 compares nonradiative decay rates from our lifetime measurements for the $^4F_{5/2}$ and $^2H(2)_{9/2}$ manifold, to those decay rates of other nonradiative transitions in Nd^{3+}:YLF cited in the literature. We restrict our attention to Nd^{3+} manifolds for the sake of clarity. In this plot, comparison is based upon Eq. (1). While there are modified forms of this equation available, as well as more sophisticated theories of multiphonon decay (as indicated in the Introduction section of this paper), the basic energy gap law of Eq. (1) is the simplest, and is sufficient for the comparisons made here. Note that all data in this plot has been temperature corrected to $T = 0$ by dividing out the temperature-dependent factor in Eq. (1), using effective phonon energy values from the literature [8]. The reference numbers to the literature are cited with each point on the graph. The solid line in the graph is a linear best fit of the data points shown.

The model of Orlovskii et al. [7] predicts that the energy gap law is not single exponential for all sizes of energy gap for a given host. In the case of a YLF host, Orlovskii et al. have observed that the energy gap law fits experimental data for energy gaps less than $\sim 2200\,cm^{-1}$ with significantly different parameters than for fitting experimental data for energy gaps greater than $\sim 2200\,cm^{-1}$ [7]. A gap of $2200\,cm^{-1}$ corresponds to about 4 effective YLF phonon energies at $560\,cm^{-1}$. (In the case of a YVO_4 host, for comparison, this change in fit parameters appears to occur near $3000\,cm^{-1}$, corresponding to about 3 phonon energies at $950\,cm^{-1}$ [12].) Fig. 7 is restricted to points with $\Delta E_{jj'} < 2250\,cm^{-1}$, so all data points there have been fitted by linear regression to get a single slope and intercept. From this slope and intercept, the B and β coefficients in Eq. (1) are $5.0 \times 10^{13}\,s^{-1}$ and $9.4 \times 10^{-3}\,cm$, respectively.

In Fig. 7, our measured nonradiative decay rate for the $^4F_{5/2}$ and $^2H(2)_{9/2}$ manifold agrees well with experimental values from the literature for other

levels, according to the energy gap law. However, there is some scatter present in the data. van Dijk and Schuurmans [9,10] have observed that nonradiative decay rates tend not to deviate more than one order of magnitude from the straight line energy gap law. We see that this observation is confirmed in Fig. 7.

4. Conclusion

The $^4F_{5/2}$ and $^2H(2)_{9/2}$ manifold of Nd^{3+} serves as a pump band in diode-pumped Nd^{3+} solid-state laser systems. In this paper, we have presented measurements of the $^4F_{5/2}$ and $^2H(2)_{9/2}$ manifold lifetime in Nd:YLF, performed using a fluorescence pump–probe technique. The technique entails populating the $^4F_{5/2}$ and $^2H(2)_{9/2}$ manifold directly through ground state absorption of a ~780 nm pump pulse. Via excited state absorption from this excited manifold, the $^2F(2)_{5/2}$ manifold of Nd^{3+} is populated with a delayed ~390 nm probe pulse. The UV fluorescence from the $^2F(2)_{5/2}$ manifold, monitored as a function of delay time between pump and probe pulses, varies linearly with each pump and probe power. Further, the wavelength peak of the spectrum of probe beam absorption matches the energy difference between the $^4F_{5/2}$ and $^2H(2)_{9/2}$ manifold and the $^2F(2)_{5/2}$ manifold. These observations are consistent with single-photon absorption of pump and probe beams as described for our experiment.

This technique, employed using short laser pulses, provides direct measurement of the picosecond lifetimes of the $^4F_{5/2}$ and $^2H(2)_{9/2}$ manifold. The 230 ± 30 ps lifetime measured agrees well with the energy gap law, based on other nonradiative lifetime measurements found for Nd:YLF in the literature for energy gaps $\Delta E_{jj'} < 2250\,cm^{-1}$.

Acknowledgements

This work and facilities were funded by the Natural Sciences and Engineering Research Council of Canada (NSERC), the Canadian Foundation for Innovation (CFI), and the Ontario Innovation Trust (OIT).

References

[1] R. Powell, Physics of Solid-State Laser Materials, Springer, New York, 1998.
[2] T. Fan, R. Byer, IEEE J. Quant. Electron. 24 (1988) 895.
[3] W. Streifer, D. Scifres, G. Harnagel, D. Welch, J. Berger, M. Sakamoto, IEEE J. Quant. Electron. 24 (1988) 883.
[4] L. Riseberg, M. Weber, in: E. Wolf (Ed.), Progress in Optics, vol. XIV, North-Holland, Amsterdam, 1976, pp. 91–159.
[5] Y. Perlin, A. Kaminskii, Phys. Stat. Sol. B 132 (1985) 11.
[6] S. Egorov, J. Skinner, J. Chem. Phys. 103 (1995) 1533.
[7] Y. Orlovskii, K. Pukhov, T. Basiev, T. Tsuboi, Opt. Mat. 4 (1995) 583.
[8] A.A. Kaminskii, Crystalline Lasers: Physical Processes and Operating Schemes, CRC Press, New York, 1996.
[9] J. van Dijk, M. Schuurmans, J. Chem. Phys. 78 (1983) 5317.
[10] M. Schuurmans, J. van Dijk, Physica B 123 (1984) 131.
[11] F. Pellé, F. Auzel, J. Alloys Comp. 300–301 (2000) 131.
[12] F. Ermeneux, C. Goutaudier, R. Moncorgé, Y. Sun, R. Cone, E. Zannoni, E. Cavalli, M. Bettinelli, Phys. Rev. B 61 (2000) 3915.
[13] S. Egorov, J. Skinner, J. Chem. Phys. 105 (1996) 10153.
[14] J. Cruz, G. Giuliani, H.M. van Driel, Opt. Lett. 15 (1990) 282.
[15] J.D. Zuegel, W. Seka, IEEE J. Quant. Electron. 31 (1995) 1742.
[16] T. Tsuboi, V. Petrov, F. Noack, K. Shimamura, J. Alloys Comp. 323–324 (2001) 688.
[17] C. Bibeau, S.A. Payne, H.T. Powell, J. Opt. Soc. Am. B 12 (1995) 1981.
[18] S.A. Payne, C. Bibeau, J. Lumin. 79 (1998) 143.
[19] H. De Leebeeck, K. Binnemans, C. Görller-Walrand, J. Alloys Comp. 291 (1999) 300.
[20] L. van Pieterson, M. Reid, R. Wegh, A. Meijerink, J. Lumin. 94–95 (2001) 79.
[21] A. Belsky, P. Chevallier, J. Gesland, N. Yu, J. Krupa, V. Makhov, P. Martin, P. Orekhanov, M. Queffelec, J. Lumin. 72–74 (1997) 146.
[22] B. Jacquier, M. Malinowski, M. Joubert, R. MacFarlane, J. Lumin. 45 (1990) 357.
[23] M. Joubert, B. Jacquier, C. Linares, R. Macfarlane, J. Lumin. 53 (1992) 477.
[24] J. Gill, Master's Thesis, McMaster University, Hamilton, Ontario, Canada, 1996.
[25] A. Kaminskii, V. Mironov, S. Bagaev, G. Boulon, Phys. Stat. Sol. B 185 (1994) 487.
[26] T. Fan, R. Byer, J. Opt. Soc. Am. B 3 (1986) 1519.
[27] Y. Orlovskii, R. Reeves, R. Powell, T. Basiev, K. Pukhov, Phys. Rev. B 49 (1994) 3821.